

THEORETICAL AND EXPERIMENTAL INVESTIGATION OF PARASITIC EFFECTS IN INDUCTION MOTOR DRIVES SUPPLIED FROM SEMICONDUCTOR INVERTERS

Stanislav BARTOŠ, Ivo DOLEŽEL, Jakub NEČESANÝ, Jiří ŠKRAMLÍK and Viktor VALOUCH

Institute of Thermomechanics AS CR, Dolejškova 5, 182 00 Prague, Czech Republic,

E-mail: {bartos, dolezel, necesaj, skramlik, valouch}@it.cas.cz

ABSTRACT

The paper deals with the numerical modeling of a pulse-width modulated voltage inverter-fed induction motor drive for the common and differential current modes. The proposed model of the drive respects the influence of the feeding cable described by the lumped or distributed parameters. The theoretical analysis is supplemented by results of relevant simulations and experiments. Evaluated are also the frequency characteristics of selected parts of the system and their contributions to its resultant harmonic spectra.

Keywords: electromagnetic interferences, semiconductor devices, inverter, induction motor, frequency characteristics.

1. INTRODUCTION

The pulse-width modulated (PWM) transistor or thyristor inverters supplying the induction motor drives often become sources of the common and differential mode currents that produce conducted and radiated electromagnetic interferences (EMI), bearing currents and decrease of the insulation lifetime. Their undesirable effects may effectively be reduced by different ways that have recently been developed, see, for example, [1]–[4].

The analysis of the amplitudes and harmonic spectra of the above parasitic currents requires adequate models of inverter-fed induction motor (IM) [5]–[12]. The paper deals with the models of a PWM voltage inverter-fed induction motor drive developed for the common and differential current modes. Both representations of the drive system take into account models of the feeding cable with lumped or distributed parameters. The theoretical analysis is supplemented by results of relevant simulations and experiments carried out on IGBT and IGCT inverters. Evaluated are also the frequency characteristics of selected parts of the system and their contributions to its resultant harmonic spectra.

2. THE BASIC MODELS

The basic arrangement of the investigated system is shown in Fig. 1.

A. Induction motor model for high frequencies

The IM can generally be modeled by an equivalent circuit consisting of several blocks connected in series. Every block contains a set of lumped parameters (see Fig. 2) determined by constrained optimization process based on the minimum difference between the calculated and measured frequency characteristics of the circuit. The circuit that we decided to use after several tests consists of two parts, which are similar in their structures but generally different in the values of particular parameters. The stator phases are modeled by two impedances Z_{v1} and Z_{v2} connected in series.

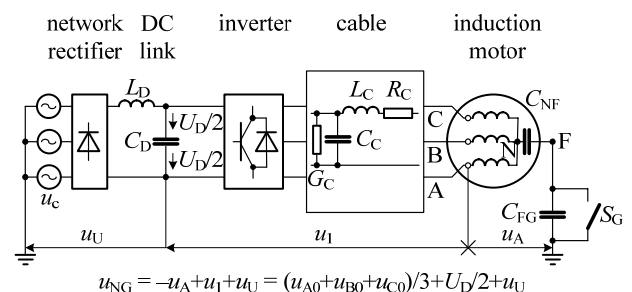


Fig. 1 The investigated drive system with an inverter, cable and IM

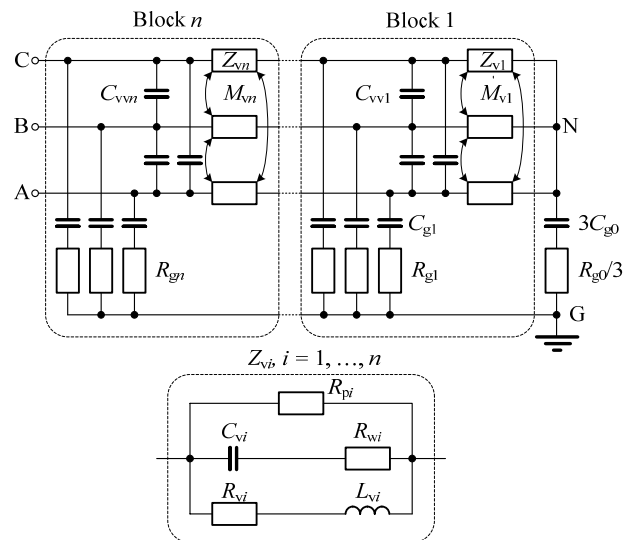


Fig. 2 The selected equivalent circuit of the induction motor

Thus, we can derive the transfer functions (IM impedances) for the common and differential modes on the basis of Fig. 2. The common mode currents flow through leakage capacitances to the earth and back to the ac power mains via the ground connection, while differential mode currents close themselves only in the phase conductors.

The influence of the mutual inductances M_{vi} may be incorporated into the transfer functions $Z_{vi}(p)$, $i=1,2$ by putting $L_{vci} = L_{vi} + 2M_{vi}$ in the common mode and $L_{vdi} = L_{vi} - M_{vi}$ in the differential mode.

Both common and differential mode transfer functions $Z_c(p)$ and $Z_d(p)$ are in the case of two blocks given by fractions containing polynomials of the seventh or eighth orders in their numerators and denominators. The order grows by four for every additional block.

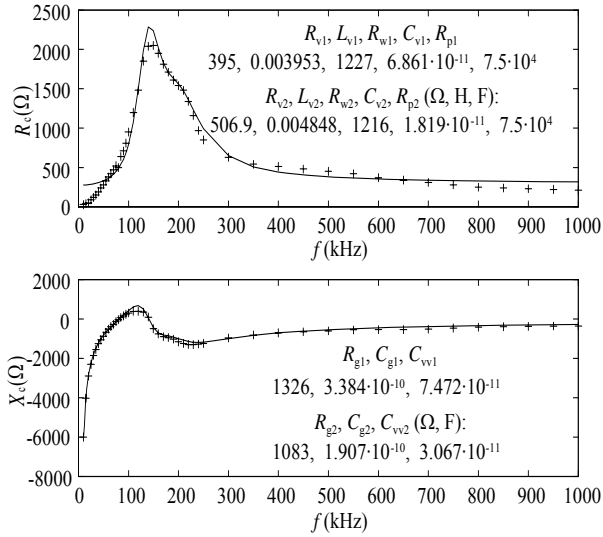


Fig. 3 Real and imaginary parts of the IM impedance in the common mode

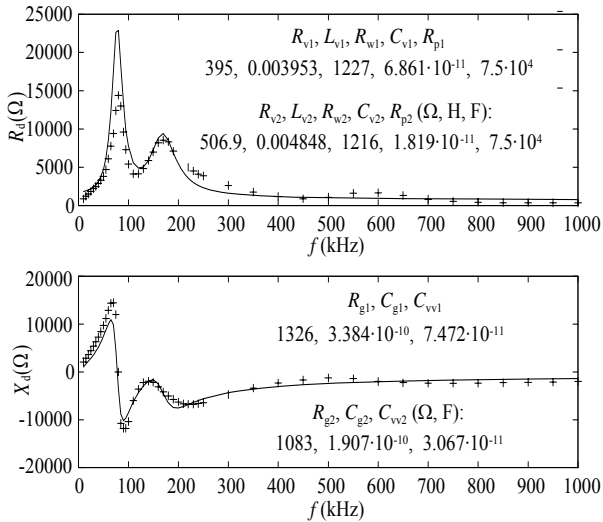


Fig. 4 Real and imaginary parts of the IM impedance in the differential mode

Fig. 3 shows both measured points and calculated frequency characteristics of the real $R_c(f)$ and imaginary $X_c(f)$ parts of the IM impedance in the common mode and Fig. 4 the same parts $R_d(f)$, $X_d(f)$ valid for the differential mode. The basic IM parameters in this case are $P=1.5$ kW, $U=380/220$ V, $f=50$ Hz, $n=1410/\text{min}$, $I=3.6/6.2$ A, $\cos\varphi=0.82$.

Note that the IM model with only one set of parameters in $Z_{vi}(p)$, $i=1,2$ was obtained, valid for both the modes. Let us also emphasize that all important resonant peaks in both models may be found by analysis of the equivalent circuit of IM shown in Fig. 2.

B. Model of feeding cable

The voltage and current distributions in a system consisting of n conductors are described by the following set of equations

$$\begin{aligned} \frac{\partial[\mathbf{u}]}{\partial x} &= -[\mathbf{R}'][\mathbf{i}] - [\mathbf{L}']\frac{\partial[\mathbf{i}]}{\partial t} \\ \frac{\partial[\mathbf{i}]}{\partial x} &= -[\mathbf{G}'][\mathbf{u}] - [\mathbf{C}']\frac{\partial[\mathbf{u}]}{\partial t} \end{aligned} \quad (1)$$

where $[\mathbf{u}]$ is a vector of the phase voltages, $[\mathbf{i}]$ a vector of the phase currents, $[\mathbf{R}']$ is a diagonal matrix containing resistances of individual conductors per unit length and $[\mathbf{L}']$, $[\mathbf{G}']$ and $[\mathbf{C}']$ are dense and symmetric matrices containing inductances, modified conductances and capacitances per unit length. The initial conditions read

$$\mathbf{u}(0,t) = \mathbf{U}(t) \quad (2)$$

while conditions at the end of the line depend on how the load is modeled and connected.

Although a number of more or less sophisticated methods were developed and studied, we used only the Fourier decomposition procedure that represents a relatively simple tool for determining the time dependence of the steady state parasitic currents. The method was incorporated into a program package written by the authors that is intended for solution of steady state and transient phenomena in systems containing feeding lines.

In case of the simplest possible representation of the cable by a lumped parameter circuit containing elements R_c, G_c, L_c, C_c , the common and differential mode transfer functions $Z_{cc}(p)$ and $Z_{dc}(p)$ of the system with the cable and motor are given by fractions with polynomials both in the numerator and denominator. These polynomials are of the order of 8/7 for Z_{cc} and 9/8 for Z_{dc} , respectively, and can be written as

$$Z_{cc}(p) = \frac{1}{3}(R_c + pL_c) + Z_c(p) \quad (3)$$

and

$$Z_{dc}(p) = 2(R_c + pL_c) + \frac{Z_d(p)}{(G_c + pC_c)Z_d(p) + 1}. \quad (4)$$

3. SIMULATIONS AND EXPERIMENTS

A great amount of simulations and measurements have been carried out for confirmation of the validity of the models and provide a deeper view into the effects. The

responses obtained on this model well correspond with the responses captured on the real drive system.

Fig. 5 shows the measured (a) and calculated (b) transient current responses of the IM (a voltage step of 10 V was applied) in the common mode. The shapes of both responses are in a good agreement (except for the very beginning).

Fig. 6 presents analogous current responses in the differential mode. The difference between the magnitudes of the measured and calculated peak values of $i_d(t)$ is in accordance with the error in $Z_d(p) = R_d + j \cdot X_d$ for the lower resonant frequency (Fig. 5). Nevertheless, the shape of the calculated response is in accordance with the measured one.

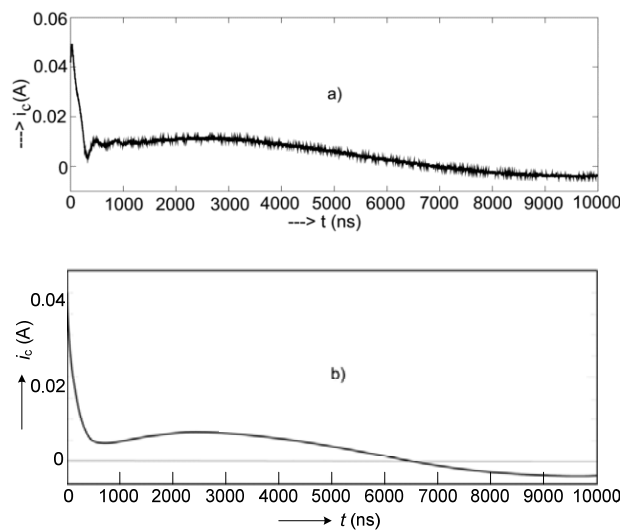


Fig. 5 Common mode current responses of IM: a) measured, b) calculated

A lot of computations based on (1), (2) were also carried out to investigate the common and differential mode current responses when the drive was fed by a series of perfectly trapezoidal voltage pulses drawn from the inverter.

Very important in this respect are the parameters of the cable. The measured values of its inductance and capacitance per unit length are almost constant within the considered range of frequencies and their average values were found to be $L'_c = 2 \cdot 10^{-6}$ H/m and $C'_c = 1.6 \cdot 10^{-6}$ F/m, respectively. The conductance G'_c per unit length is far from being constant and grows with frequency, but as in comparison with $\omega C'_c$ is always too small, its value was taken 10^{-8} S/m. Finally R'_c (Ω /m) is strongly dependent on frequency and for the mathematical model it was approximated by function

$$R'_c(f) = R'_{c0} + kf^2 \quad (5)$$

where relevant measurements provided values $R'_{c0} = 0.02 \Omega/\text{m}$ and $k = 0.28 \cdot 10^{-12} \Omega\text{m}^{-1}\text{s}^{-2}$.

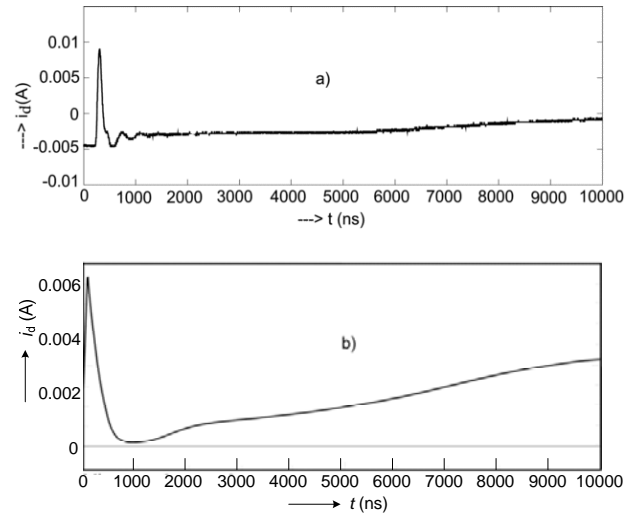
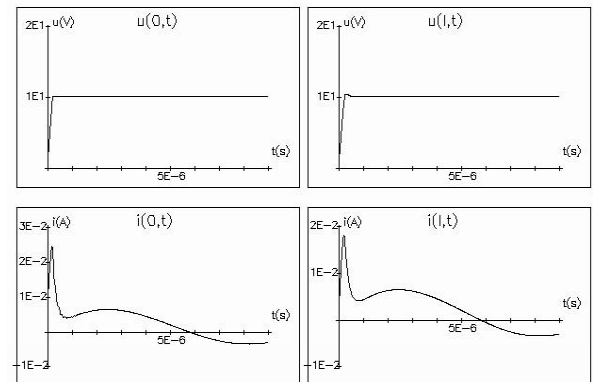


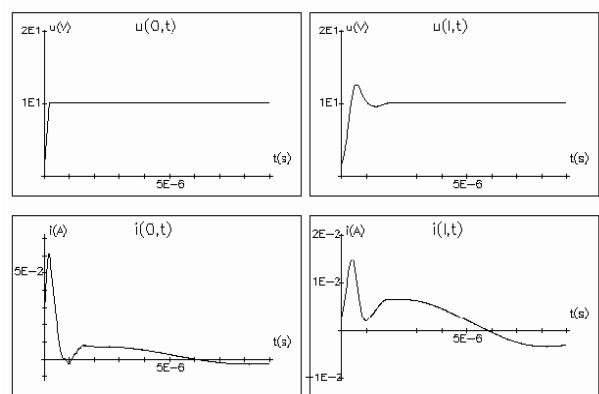
Fig. 6 Differential mode current responses of IM: a) measured, b) calculated

t1= 0.20mics, t2= 24.80mics, t3= 0.20mics, t4= 24.80mics, U= 10.0V, R = 0.02000hm/m, L = 2.0000micH/m, C = 0.1600nF/m, G = 10.0nS/m, l= 1.0m,



a) length of the cable $l_c = 1$ m

t1= 0.20mics, t2= 24.80mics, t3= 0.20mics, t4= 24.80mics, U= 10.0V, R = 0.02000hm/m, L = 2.0000micH/m, C = 0.1600nF/m, G = 10.0nS/m, l= 10.0m,



b) length of the cable $l_c = 10$ m

Fig. 7 Calculated voltage and common mode current responses in a system with feeding cable and IM

While Fig. 7a) shows the steady state values of voltage and common mode current responses at the beginning (left hand side) and the end (right hand side) of the cable of the

length of 1 m, Fig. 7b) presents similar values for the cable of length of 10 m. The comparison of the figures shows the overvoltages at motor terminals are higher, as a result of wave phenomena, and the current peaks at the inverter terminals are more pronounced due to cable leakage currents, for the longer cable.

Fig. 8 compares the calculated (the number of the Fourier expansion terms being 500) and measured transient common mode current responses in a system with the feeding cable of length 10 m and induction motor.

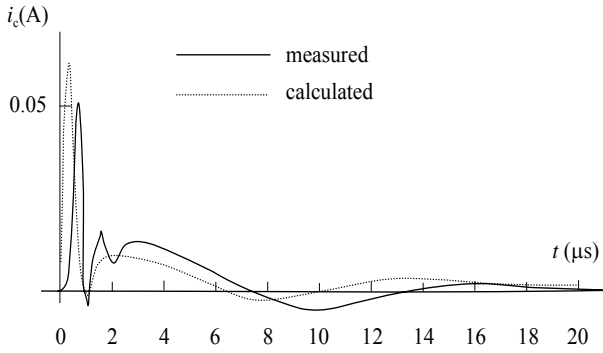


Fig. 8 Calculated and measured current response in the common mode (system with the feeding cable of length 10 m and IM)

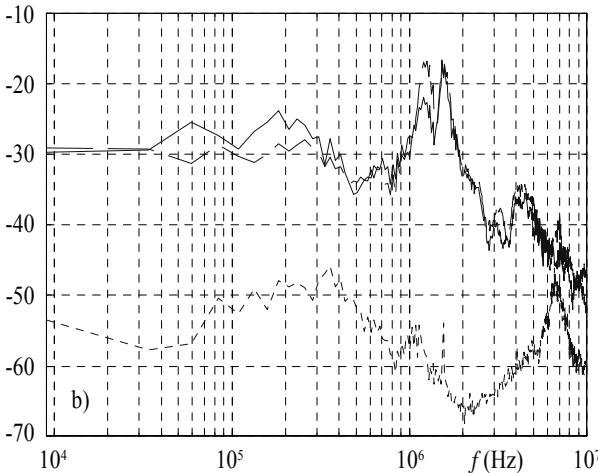
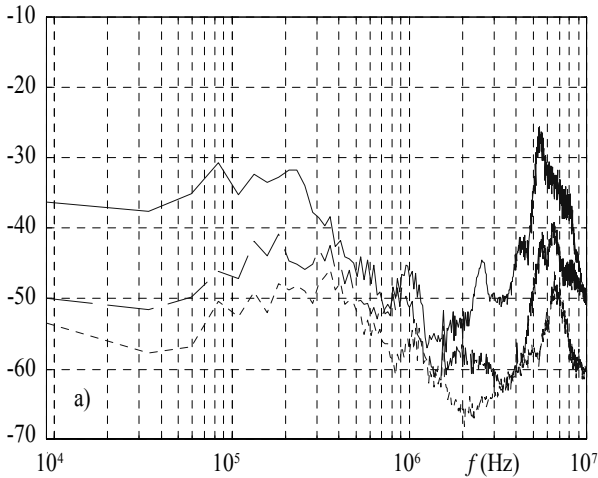


Fig. 9 Common mode interference spectra for a) $l_c = 2$ m, b) $l_c = 30$ m

Fig. 9 shows the common mode interference spectra detected at the measurement point at the LISN and expressed in the double logarithmic representation for two different lengths of the feeding cables ($l_c = 2$ m and 30 m). Three characteristics are depicted, namely for only the inverter in operation (dotted lines), the IGBT inverter with the feeding cable (dashed lines) and for the inverter feeding the IM through the cable (full lines). By comparing the interference spectra for different lengths of the cable and different parts of the system we can evaluate impacts of these individual subsystems of the drive.

Two main peaks (around 350 kHz and 6.5 MHz) may be distinguished at the frequency spectrum for the inverter working alone without any load. After comparing the curves in the two figures we can see that the longer is the cable, the higher is the level of the common mode interference (dashed lines), while for the longer cable the spectra measured without and with the induction machine (Fig. 9b) are almost identical.

The reason is that with growing length of the cable the current flowing through the stray capacitances of the cable to ground increases. For a certain length of the cable the contribution of the IM leakage current to the total current is almost negligible, except for the range of lower frequencies (below a few hundreds of kHz). It is clearly visible that the character of the spectra (full lines) between 70 and 300 kHz is practically the same regardless the lengths of cables feeding the IM. It indicates that this part characterizes the IM. On the contrary, the second dominating part of the characteristics (around 5.5 and 1.5 MHz) depends on the cable length (2 and 30 m).

As a matter of fact, power switching devices exhibit permanent improvement which can be demonstrated e.g. by the successive development of GTOs into IGCTs. In general, the objective was an increase in the device ratings, especially in terms of the repetitive peak blocking voltage (nowadays up to $V_{DRM} = 4500$ V), the maximum controllable turn-off current (nowadays up to $I_{TGQM} = 4000$ A) and the device switching frequency. The IGCT is based on the principle that is called the hard-driven turn-off process, which is known also as unity-gain turn-off.

Fig. 10 compares the voltage front edges produced by an IGCT inverter to voltage front edges produced by the IGBT inverter. For this comparison, however, inverters with the same dc supply voltage were not at our disposal. The IGBT inverter was made up of a MITSUBISHI module and the provided dc feeding voltage was 310 V. The IGCT inverter, on the other hand, was supplied by 550 V. The supplied motor was an IM of the type TB 702 with rated values 85 kW, 75 Hz, 2214 rpm, 133.8 A.

We see that the voltage front edges at both the IGBT and IGCT inverters have similar steep slopes and, although the switching times at the IGCT-based inverters are longer than those at the IGBT inverters, it may be expected that these inverters will produce also similar voltage waves traveling along the cables connecting the inverters and ac motors and resulting overvoltage phenomena, see Fig. 11. To eliminate solitary, accidental, and abnormal waveforms, two characteristic waveforms (samples) measured very close to the inverter and two characteristic samples measured very close to the motor were selected for the

harmonic analysis. The figure demonstrates that the presence of the cable results in overvoltages at the IM terminals.

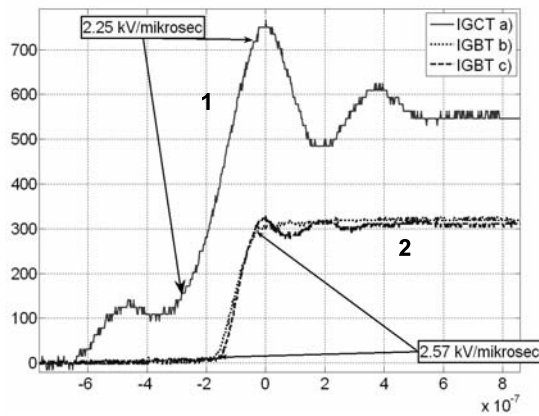
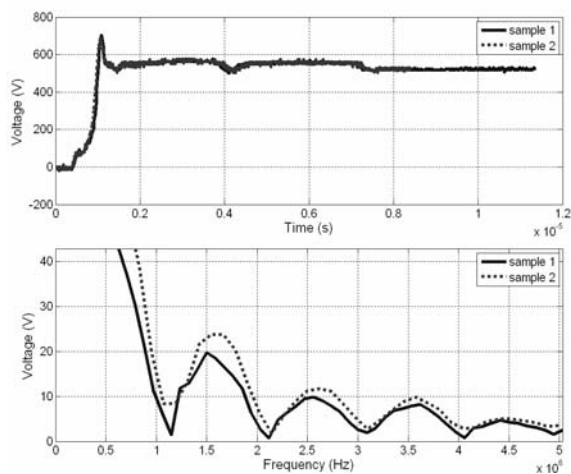
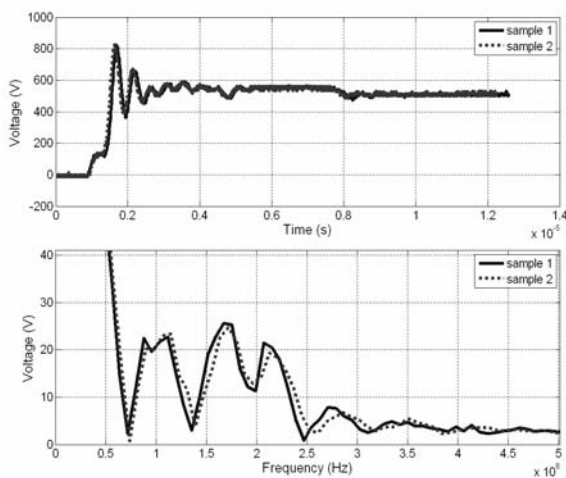


Fig. 10 Comparison of voltage front edges, the voltage across the minus dc input terminal and any of ac outputs, cable length 3m

1. IGCT inverter: separate phase cables, point of measurement 1 m distant from the inverter,
2. IGBT inverter, 3-phase cable employed



a) close to IGCT inverter



b) close to IM

Fig. 11 Voltage-time, voltage-frequency relationships (IGCT inverter, cable 10 m long), measured at two different positions

We have found that the results and experience referred so far are very useful at the development and testing of some drives of vehicles for city mass transport from the point of view of EMI. In addition to conducted high frequency parasitic currents also radiated EMI produced by the drives of vehicles (tramways and trolleybuses) were calculated and measured.

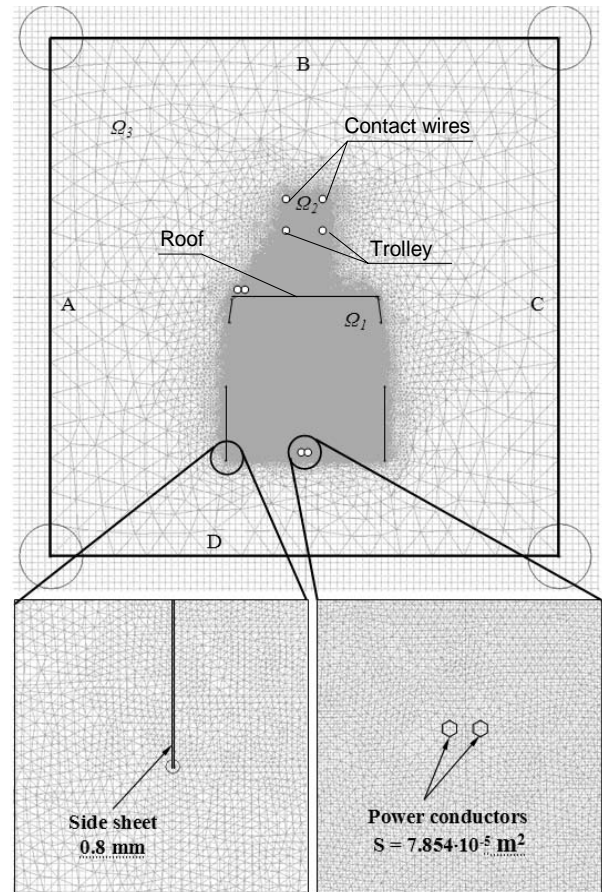


Fig. 12 Calculation of magnetic field inside and outside the trolleybus TR21. Mesh with details: 379807 nodes

Figs. 12 and 13 show the examples of results gained when modeling magnetic field inside and outside the trolleybus TR21. The computations were carried out for various working regimes and for application of two different power switching semiconductor devices (IGBTs, IGCTs). The influence on near low-current and telecommunication systems was of our interest, too. The computation of the magnetic field was performed by the professional FEM-based program QuickField. The results were compared with the values measured and those given by the corresponding standards.

Figs. 14 and 15 show the examples of the measured levels of EMI in the city transport enterprises in Czech towns Hradec Králové and Plzeň. It is important to note that at Hradec Králové a trolleybus with IGCT devices was tested, see Fig. 14. The EMI background there was influenced by other trolleybuses, which were operating at the same time. The EMI of a tramway equipped with IGBT inverters was measured at Plzeň, see Fig. 15. The tramway was a prototype under test operation and no other similar tramways were connected to the overhead contact

system. To increase the objectivity, many measurements at various localities were carried out.

The results summarized in Figs. 12–15 were helpful when suggesting measures for the reduction of EMI.

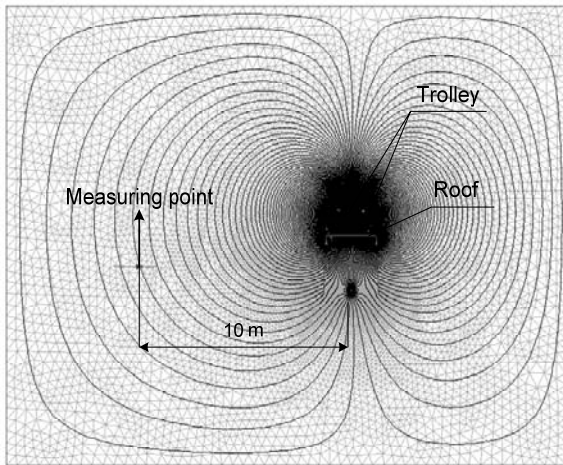


Fig. 13 Contours of calculated magnetic field strength inside and outside the trolleybus TR21

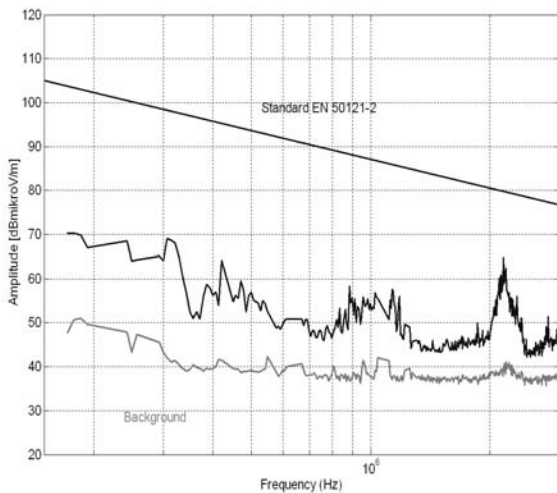


Fig. 14 Values of EMI obtained from the analyzer E7401A at Hradec Králové (trolleybus TR21). The measurements were performed in accordance with the demands (distance of the antenna, etc.) specified in Standard EN 50121-2

4. CONCLUSION

The equivalent models of the feeding cable and induction motor appropriate for the determination of stray current disturbances in the common and differential modes have been suggested. The frequency characteristics of selected parts of the system and their contributions to the resultant harmonic spectra have been evaluated as well.

The responses obtained on this model well correspond with the responses captured on the real drive system. This holds even at the very beginning of the transients, where the variables (mainly currents) are characterized by steep changes (peaks) and high frequencies.

The IGCT inverters have to be expected to produce similar voltage waves traveling along the cables connecting the inverters and ac motors and other phenomena as

those produced by the IGBT inverters, even when the IGCT total switching times are substantially longer.

The paper summarizes also the most important experimental results. These results were obtained both in the laboratory (experimental operation of the IGBT and IGCT inverters feeding a 3-phase induction machine) and during the practical tests of these switching devices in vehicles of city mass transportation.

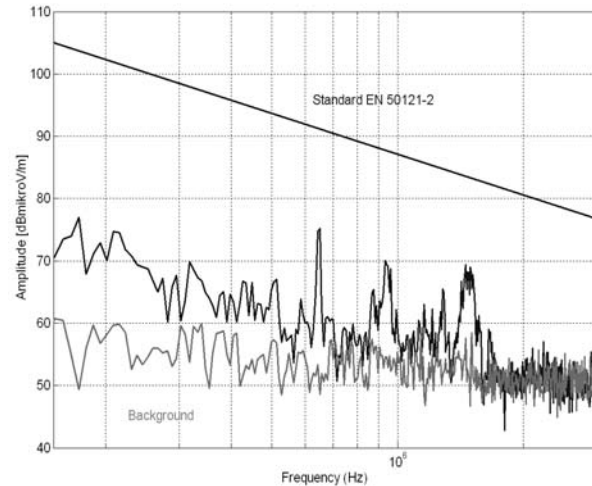


Fig. 15 Values of EMI obtained at Plzeň (a tramway equipped with IGBT inverters)

ACKNOWLEDGEMENT

The financial supports of the Grant Agency of the Czech Republic (Project No. 102/06/0112) and the Academy of Sciences of the Czech Republic (Institutional Research Plan Z20570509 of the Institute of Thermomechanics, v.v.i.) are gratefully acknowledged.

REFERENCES

- [1] Van der Broeck, H., Loeff, Chr.: Use of LC Filters in Hard Switching PWM Inverter Drives. Proc. EPE'95, Seville, Spain, 1995, pp. 1536–1541.
- [2] Von Jouanne, A., Rendusara, D. A., Enjeti, P. N., Gray, J. W.: Filtering Techniques to Minimise the Effects of Long Motor Leads on PWM Inverter-Fed AC Motor Drive Systems. IEEE Trans. IA 32, 1996, No. 4, pp. 919–925.
- [3] Ogasawara, S., Akagi, H.: Modelling and Damping of High-Frequency Leakage Currents in PWM Inverter-Fed AC Motor Drive Systems. IEEE Trans. IA 32, 1996, No. 5, pp. 1105–1113.
- [4] Mutoh, N., Ogata, M.: New Methods to Control EMI Noises Generated in Motor Drive Systems, IEEE Trans. IA 40, 2004, No.1, pp. 143–152.
- [5] Persson, E.: Transient Effects in Application of PWM Inverters to Induction Motors. IEEE Trans. IA 28, 1992, No. 5, pp. 1095–1101.
- [6] Cacciato, M., Consoli, A., Scarcella, G., Testa, A.: Effects of PWM Techniques on Common Mode Cur-

- rents in Induction Motor Drives. Proc ISIE'97, Guimarães, Portugal, 1997, pp. SS212–SS217.
- [7] Consoli, A., Oriti, G., Testa, A., Julian, A. L.: Induction Motor Modeling for Common Mode and Differential Mode Emission Evaluation. Proc. 31st IAS Annual Meeting, San Diego, USA, 1996, pp. 595–599.
- [8] Grandi, G., Casadei, D., Reggiani, U.: Equivalent Circuit of Mush Wound AC Windings for High Frequency Analysis. Proc. ISIE'97, Guimarães, Portugal, 1997, pp. SS201–SS206.
- [9] Kerkman, R. J., Leggate, D., Skibinski, G. L.: Drive Modulation and Cable Parameters on AC Motor Transients. IEEE Trans. IA 33, 1997, No. 3, pp. 722–729.
- [10] Akagi, H., Tamura, S.: A Passive EMI Filter for Eliminating Both Bearing Current and Ground Leakage Current From an Inverter-Driven Motor. IEEE Trans. PE 21, 2006, No. 5, pp. 1459–1469.
- [11] Boglietti, A., Carpaneto, E.: An Accurate Induction Motor High-Frequency Model for Electromagnetic Compatibility Analysis. Electric Power Components and Systems, Taylor & Francis, Vol. 29, 2001, pp. 191–209.
- [12] Lai, J. S., Huang, X., Pepa, E., Chen, S., Nehl, T. W.: Inverter EMI Modeling and Simulation Methodologies. IEEE Trans. IE 53, 2006, No.3, pp. 736–744.

Received March 31, 2008, accepted September 29, 2008

BIOGRAPHIES

Assoc. Prof. Stanislav Bartoš (1935) graduated from the Faculty of Electrical Engineering of the Czech Technical University, Prague in 1958. He has 21 year experience in heavy industry (development engineer in power electronics applications). Since 1981 he has been working with the Institute of Electrical Engineering of the Academy of Sciences of the Czech Republic (fused with the Institute of Thermomechanics two years ago) in the field of voltage source inverters, IGBTs, IGCTs, ETOs. From 2002 to 2005 he was head of the Department of Power Electronics, currently he is a scientific advisor. He is an author or co-author of about 40 scientific papers.

Prof. Ivo Doležel (1949) obtained his Eng. degree from the Faculty of Electrical Engineering (Czech Technical University in Prague) in 1973 and after 28 years in the Institute of Electrical Engineering of the Academy of Sciences of the Czech Republic he returned back to the Czech Technical University. His interests are aimed mainly at electromagnetic fields and coupled problems in heavy current and power applications. He is an author or co-author of one monograph, about 300 papers and several large program packages.

Jakub Nečesaný, PhD. (1978) obtained his Eng. degree from the Faculty of Electrical Engineering (Czech Technical University in Prague) in 2004 and PhD degree from the same university in 2007. Since 2002 he has been working at the Institute of Electrical Engineering of the Academy of Sciences of the Czech Republic (fused with the Institute of Thermomechanics in 2006). He is interested in numerical modelling and computing. He is an author or co-author of about 10 scientific papers.

Prof. Viktor Valouch (1947) finished his studies at the Faculty of Electrical Engineering of the Czech Technical University in 1972 (MSc) and degree PhD he received in 1976 from the same CTU. In 1975 he joined the CKD Semiconductors where he dealt with problems connected with induction motor drives fed from inverters. Since 1977 he has been working with the Institute of Electrical Engineering of the Academy of Sciences of the Czech Republic (fused with the Institute of Thermomechanics two years ago). His present research activities are concentrated on microprocessor-based control systems, ac drives with variable speed, static inverters and active power filters. He is an author or co-author of about 170 papers in periodical journals and conference proceedings and also 3 patents.

Jiří Škramlík, PhD. (1956) finished his studies at the Faculty of Electrical Engineering of CTU in Prague in 1982. In 1993 he joined the Institute of Electrical Engineering of the Academy of Sciences of the Czech Republic (fused with the Institute of Thermomechanics two years ago) as a research engineer. Now he is a researcher with the Institute of Thermomechanics. He has dealt with problems of the pulse width modulation in the voltage inverters for induction motors and active power filters, and utilisation of the digital signal processors. He is an author or co-author of about 40 papers and 4 patents.